University of Kent

Kent Academic Repository

Njogu, Peter, Sanz-Izquierdo, Benito, Chen, Zhijiao and Parker, E.A. (2023) ***3D Frequency Selective Surface Displacement Sensor using Complementary Dielectrics.*** **IEEE Sensors Journal . p. 1. ISSN 1558-1748.**

Downloaded from
https://kar.kent.ac.uk/102050/ The University of Kent's Academic Repository KAR

The version of record is available from
https://doi.org/10.1109/jsen.2023.3289777

This document version
Author's Accepted Manuscript

DOI for this version
https://doi.org/10.22024/UniKent/01.02.102050.3405583

Licence for this version
CC BY (Attribution)

Additional information
For the purpose of open access, the author has applied a CC BY public copyright licence to any Author Accepted Manuscript version arising from this submission.

Versions of research works

Versions of Record
If this version is the version of record, it is the same as the published version available on the publisher's web site. Cite as the published version.

Author Accepted Manuscripts
If this document is identified as the Author Accepted Manuscript it is the version after peer review but before type setting, copy editing or publisher branding. Cite as Surname, Initial. (Year) 'Title of article'. To be published in ***Title of Journal*** , Volume and issue numbers [peer-reviewed accepted version]. Available at: DOI or URL (Accessed: date).

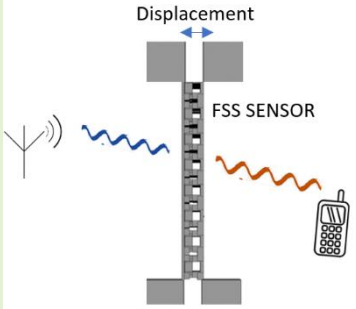
Enquiries
If you have questions about this document contact ResearchSupport@kent.ac.uk. Please include the URL of the record in KAR. If you believe that your, or a third party's rights have been compromised through this document please see our Take Down policy (available from https://www.kent.ac.uk/guides/kar-the-kent-academic-repository#policies).

This article has been accepted for publication in IEEE Sensors Journal. This is the author's version which has not been fully edited and content may change prior to final publication. Citation information: DOI 10.1109/JSEN.2023.3289777

3D Frequency Selective Surface Displacement Sensor using Complementary Dielectrics

Peter Njogu, Benito Sanz-Izquierdo, Zhijiao Chen and E.A. Parker

***Abstract*— A novel displacement sensor using a frequency selective surface (FSS) with a removable substrate complement is proposed. The new concept sensor is based on modifying the effective permittivity of the FSS when the substrate complement is gradually withdrawn. The change in the effective permittivity produces a change in capacitance, and thus in the resonant frequency. The FSS consists of an array of square loops elements in a square lattice. A 3D convoluted version of the FSS sensor improves the angle of incident behavior and increases the displacement range. The dielectric layers of the 3D FSS sensor were 3D printed while the metal layers were painted using silver conductive paint. The transmission response, S_{21}, has been employed as the validation parameter. The proposed sensor operates in a frequency range between 2.0 GHz and 2.8 GHz and has achieved a 0.052 GHz/mm sensitivity and 12 mm dynamic range and has a dimension of 207mm by 207mm. The sensor is passive, compact, inexpensive, and easy to operate. The envisaged application is the wireless detection of structural movement, which can be critical in civil structures such as bridges or buildings or earthquake monitoring.**



***Index Terms*— Frequency Selective Surface (FSS), displacement, sensor, periodicity**

I. Introduction

Frequency selective surfaces (FSS) are typically periodic arrays of conductive elements on dielectric materials that exhibit specific transmissive or reflective frequency responses when the electromagnetic energy impinges. Their frequency response depends on the spacing between the periodic elements, their geometry, the dielectric substrate properties, its thickness, and the local environment [1] and [2]. FSS behave as spatial filters to certain frequencies of impinging electromagnetic radiation.

The filtering properties of FSS enable exploitation of the electromagnetic responses, i.e., reflection and transmission properties, resonance frequency and Q-factor which depends on the unit cell geometry and the dielectric material characteristics. Alterations of parameters such as layering the dielectric structure [3] or composition [4] affect the response of the FSS. These FSS filtering properties enable its application in advanced antenna systems and technology e.g., offset reflector antennas [5], absorbers [6], radomes [7], Butler matrix [8]. RF shielding [9], beam switching and steering [10] [11]. FSS and meta-materials have been proposed for applications in strain [12], remote [13], chemical liquid [14], thin film [15], CO_2 [16], bridge columns structural health monitoring [17] Biochemical [18] and corrosion [19] sensing.

Displacement can be detected using a variety of sensors, the most common being based on resistive, capacitive, inductive, ultrasonic [20] and optical principles [21]. In the microwave spectrum, displacement sensors employing transmission line structures have been developed [22] - [24]. EBG based displacement sensors have also been investigated [25], [26]. Compared with most of those displacement sensors, FSS based sensors have the advantage of being passive, scalable, and able to operate remotely e.g., remote structural health monitoring using FSS-based sensors has been proposed [27]. This sensor involves an FSS tearing or deforming to indicate a structural health problem. More specifically on displacement sensors, a wireless two-dimensional lateral sensor using bilayer graphene-based FSS is described in [28], while that presented in [29] uses an antenna coupling in the near field with two split-ring metamaterials that are gradually moved apart.

FSS exists in many profiles [1][30]. They are typically planar (2D), but some are also three-dimensional [31], [32]. 3D FSS has been developed for improved filter selectivity [33], [34] and some offer improved wave angle of incidence stability [35], [36]. However, very high angle stability has mostly been achieved on 2D FSS [37], [38] using convoluted techniques [39]. The question that arises is whether 3D FSS structures have advantages over 2-dimensional ones.

In this paper, a novel FSS-based displacement sensor is proposed using complementary dielectric structures. The design has two main components: an FSS and a dielectric complement. The parts are arranged so the dielectric complement is retractable from the FSS along the z-plane. The sensing function occurs through variation of the effective permittivity as the dielectric complement retracts. This changes the capacitance of the FSS, which alters the resonance frequency. A 3D convoluted FSS design is proposed to improve the angle of incidence and increase the displacement range. The

This paragraph of the first footnote will contain the date on which you submitted your paper for review. It will also contain support information, including sponsor and financial support acknowledgment. For example, "This work was supported in part by the U.S. Department of Commerce under Grant BS123456."

Authors Peter Njogu, Benito Sanz-Izquierdo and E.A. Parker are with the University of Kent, School of Engineering and Digital Art, Canterbury CT2 7NZ, UK (e-mail: pmn20@kent.ac.uk; b.sanz@kent.ac.uk; e.a.parker@kent.ac.uk). Zhijiao Chen is with Beijing University of Posts and Telecommunications Beijing, China (email: z.chen@bupt.edu.cn)

XXXX-XXXX © XXXX IEEE. Personal use is permitted, but republication/redistribution requires IEEE permission.
See http://www.ieee.org/publications_standards/publications/rights/index.html for more information.
Authorized licensed use limited to: UNIVERSITY OF KENT. Downloaded on July 14,2023 at 13:16:53 UTC from IEEE Xplore. Restrictions apply.
© 2023 IEEE. Personal use is permitted, but republication/redistribution requires IEEE permission. See https://www.ieee.org/publications/rights/index.html for more information.

This article has been accepted for publication in IEEE Sensors Journal. This is the author's version which has not been fully edited and content may change prior to final publication. Citation information: DOI 10.1109/JSEN.2023.3289777

3D convoluted FSS sensor has been fabricated, and its transmission response measured. The FSS sensor operates at about 2.5 GHz with a broad range of frequencies in relation to the displacement distance of the complement dielectric. The proposed sensor is adaptable and can be adjusted in size by increasing or decreasing the number of cells. It is passive and does not require internal batteries. The dielectric layers of the FSS were fabricated using fused filament fabrication (FFF), a method that enables the creation of intricate 3D objects [40].

The rest of this paper is organized as follows. Section II introduces the basic principle of the FSS sensor and describes the theoretical concept. Section III describes the 3D convoluted FSS sensor. Section IV provides details of the fabrication and measurements of the design, and finally, section IV is the discussion of the performance of the sensor and conclusion.

II. FSS Displacement Sensor Concept

A. Design of the basic FSS and Dielectric Complement

FSS structures are known to be sensitive to their surrounding materials as well as the substrate characteristics, the feature that has been exploited to develop the proposed sensor.

The square loop FSS element offers dual polarization and good angle of incidence behavior [2] and was adopted in the development of the proposed sensor, Fig. 1. A 21.7 mm square loop is set on the 26 mm square unit cell, Fig. 1(a), was designed to fit into a complement structure, Fig.1 (b), as shown in Fig. 1(c). Fig. 1(d) illustrates a withdrawn state of complement while Fig. 1(e) illustrates a two cells array of the design. A Polylactic acid (PLA) substrate of relative permittivity, ε_r, 2.4 and loss tangent ($\tan\delta$) of 0.01 [41] was used. The substrate thickness was 6 mm. The rest of the dimensions are given in Table I. The design was simulated using Floquet port analysis in CST Microwave Studio™.

The transmission response of the FSS sensor is shown in Fig. 2. The FSS without the complement resonated at 4.4 GHz with a frequency shift of 5% at TE 45°, and 1.8% at TM 45° wave incidence. With the complement, the FSS resonated at 3.5 GHz with a frequency shift of 2.9% at TE45°, and 2.0% at TM45°.

A further study of the resonant frequency of the FSS sensor for a range of displacement distances, z, of the complementary structures (Fig. 1(d)), was conducted, and the result is shown in Fig. 3. The substrate complement was withdrawn in the z-plane direction at intervals Δz of 2 mm, ranging from 0 mm (Fig. 1(d)) to 10 mm. The sensor's response is linear up to 4 mm, after which it flattens as the complement moves out of FSS. This initial concept has a low displacement range.

B. The Operation Principle

A typical bandstop FSS can be modelled as an equivalent circuit theory [42] and [43]. Adjacent square loops of FSS act capacitively while the metallic conductor strip is equivalent to an inductor, creating a series LC resonance circuit, as shown in Fig. 4. The resonance frequency of this circuit is expressed as:

$$f = \frac{1}{2\pi\sqrt{LC}} \tag{1}$$

where L is the inductance created by the conductors of the square loops while C is the capacitance between adjacent loops. Capacitance, C, can be approximated using (2) [43]:

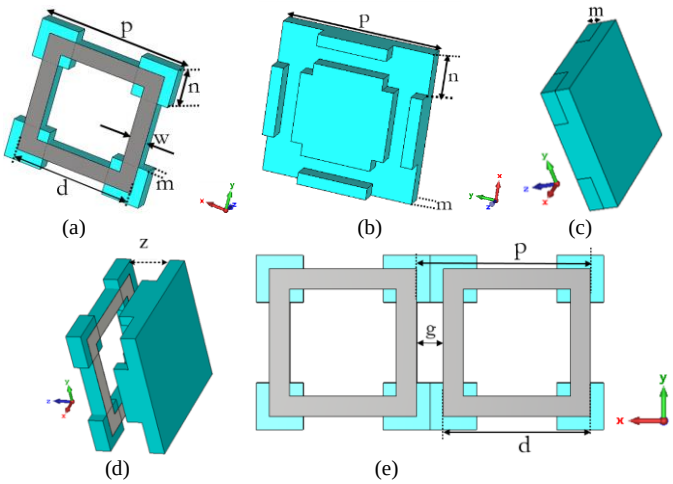


Fig. 1 The concept: the (a) FSS (b) substrate complement (c) FSS plus complement (d) complement substrate withdrawal (e) Two-cells array

TABLE I: DIMENSION OF THE INITIAL CONCEPT FSS

Dimension	p	w	m	n	d
Value, (mm)	26	2	3	7	21.7

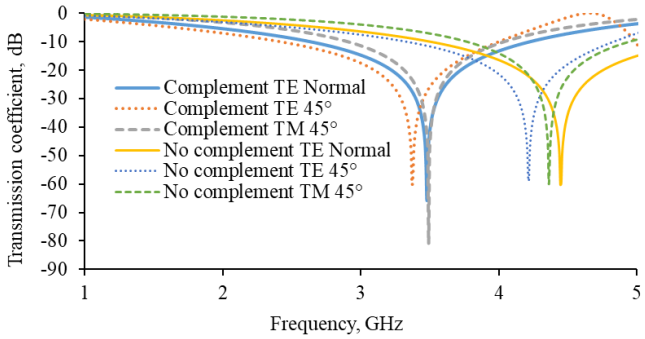


Fig. 2 S_{21} of the FSS displacement sensor with and without complement

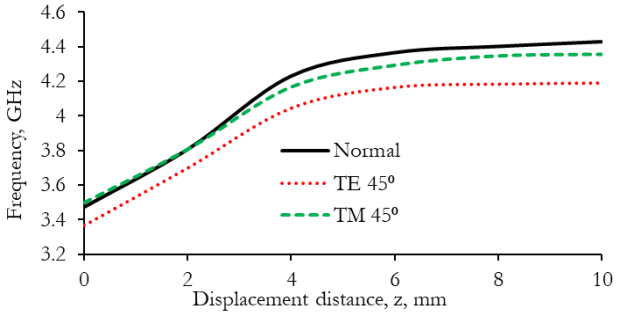


Fig. 3 Simulated resonance frequency, f, versus substrate complement displacement distance, z for the 2D sensor

$$C = \varepsilon_r \varepsilon_{eff} \frac{2d}{\pi} In\left(cosec\left(\frac{\pi g}{2d}\right)\right) \tag{2}$$

where ε_{eff} and ε_r are effective permittivity and permittivity respectively, d is the loop dimension and g are the conductor strip separation. The sensor operating principle involves variation of the capacitance of the LC circuit as the dielectric complement retracts out of the FSS structure, as illustrated in Fig. 5. The initial state, Fig.5 (a), has the FSS symmetrically embedded in the dielectric substrate of permittivity ε_r. In this case, the effective permittivity can be approximated to ε_r as the substrate is moderately thick and square loops are used [44]. When the dielectric complement is retracted from the FSS, the

Authorized licensed use limited to: UNIVERSITY OF KENT. Downloaded on July 14,2023 at 13:16:53 UTC from IEEE Xplore. Restrictions apply.
© 2023 IEEE. Personal use is permitted, but republication/redistribution requires IEEE permission. See https://www.ieee.org/publications/rights/index.html for more information.

This article has been accepted for publication in IEEE Sensors Journal. This is the author's version which has not been fully edited and content may change prior to final publication. Citation information: DOI 10.1109/JSEN.2023.3289777

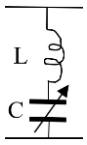


Fig. 4 Equivalent circuit of the FSS sensor

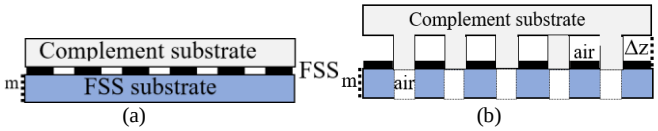


Fig. 5 Cross-sectional view of the sensor at withdrawal distance z at (a) zero (b) 4 mm

effective permittivity of the structure decreases. This decreases the capacitance of the FSS. The effective permittivity for a fully retracted complement substrate, Fig. 5(b) could be approximated to a substrate with half dielectric and half air. Thus, the effective permittivity is:

$$\varepsilon_{eff} = \frac{\varepsilon_r + 1}{2} \tag{3}$$

The gradual change between these two states (Fig. 5(a) and Fig. 5(b)) is expected to be linear, which leads to the equation:

$$\varepsilon_{eff} = \varepsilon_r + \frac{(1-\varepsilon_r)}{2m} z \tag{4}$$

where z is the displacement along the z axis and m is the height of the FSS. Equation (4) is only valid for the linear part of the sensor which is intermediate to Fig.5(a) and Fig. 5 (b), i.e., for z between 0 and 3 mm (Fig.3) of the initial sensor in Fig. 1.

In fact, it is possible to obtain a more accurate equation for the change in effective permittivity for the structure in Fig (1) using the ratios between the resonant frequency at any z, f_z , and the frequency for z = 0, f_1 and the ratio between ε_{eff} at any point z, and ε_r (ε_{eff} at z = 0) This ratio can be obtained using (1) and (2), considering that L, g, and d, are constants. Using these ratios, ε_{eff} for any frequency can be calculated as:

$$\varepsilon_{eff} = \left(\frac{1}{\left(\left(\frac{f_z}{f_1} \right)^2 \right)} \right) \varepsilon_r \tag{5}$$

Applying this equation to the values for the frequencies in Fig. 3, the value of ε_{eff}as a function of z can be obtained as shown in Fig. 6. The equation for the effective permittivity for the linear part (0 < z < 4) of the graph is:

$$\varepsilon_{eff} = 2.4 - 0.1947z \tag{6}$$

It should be noted that the linear part extends 1mm (to z = 4mm) from that predicted earlier. Nevertheless, (6) is consistent with (3) and (4). For example, at 4 mm, ε_{eff} for the half loaded FSS from (3) is just 5% higher than that using (6). The differences are probably due to the non-uniformity of the dielectric material extracted during displacement and errors in the initial assumption that the substrate might be sufficiently thick to be considered as fully loaded with dielectric [44].

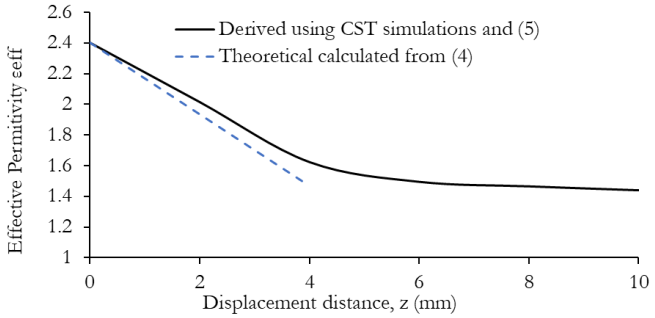


Fig. 6 Effective permittivity for displacement distance, z

III. 3D Convoluted FSS Displacement Sensor

A. 3D Convoluted design

To improve the sensor's angular response and increase the displacement range, the initial square loop (Fig.1) was extended in the z axis, resulting in the 3D square loop, Fig. 7(a). The substrate complement for this FSS is shown in Fig. 7 (b). Fig. 7(c) shows when the two parts joined together, and Fig. 7(d) when they are slid out. The sensor was optimized to operate at a starting frequency with complement of about 2.16 GHz. The final dimensions are given Table II. The square loop array was arranged in a square periodicity of 26 mm. In Fig. 7(d), z is the displacement distance of the complement substrate from of the FSS, h is the height of the FSS.

The simulation's transmission coefficients of the FSS at normal incidence, TE 45° and TM 45° angles of incidence are shown in Fig. 8, for the FSS with and without the substrate complement. The FSS without the complement resonated at 2.8 GHz with a frequency shift of 1.2% at TE 45°, and 0.7% at TM 45°. When FSS is coupled together with the complement resonance occurred at 2.16 GHz with a frequency shift of 0.5% at TE 45° and 0.15% at TM 45°.

B. 3D Convoluted FSS Sensor Parametric Analysis

The surface current on the FSS is shown in Fig. 9. As with ordinary square loops, the current density is maximum at the center of the sides of the loop. A study of displacement sensing was carried out by gradually withdrawing the substrate complement along the z axis (Fig. 7(d)). Fig. 10 shows the effect of displacement on the resonant frequency, and the equivalent effective permittivity calculated using (5). The response is mainly linear up to about 12 mm. The transmission coefficients for various z for the linear part of the sensor ($0 \leq z \leq 10$mm) are shown in Fig. 11. As the displacement distance (z) changes from 0 mm to 10 mm, the resonance frequency increases from 2.16 GHz to 2.67 GHz. The frequency response follows the linear function:

$$f = 0.052z + 2.1481 \tag{7}$$

The sensitivity (S) of the sensor [28], is the slope of the linear equation (0.052/mm) as given by:

$$S = \frac{\Delta f_z}{\Delta z} \tag{8}$$

Authorized licensed use limited to: UNIVERSITY OF KENT. Downloaded on July 14,2023 at 13:16:53 UTC from IEEE Xplore. Restrictions apply.
© 2023 IEEE. Personal use is permitted, but republication/redistribution requires IEEE permission. See https://www.ieee.org/publications/rights/index.html for more information.

This article has been accepted for publication in IEEE Sensors Journal. This is the author's version which has not been fully edited and content may change prior to final publication. Citation information: DOI 10.1109/JSEN.2023.3289777

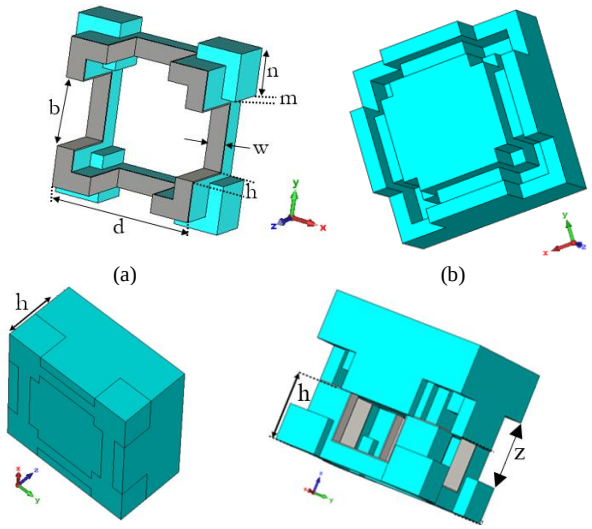


Fig. 7. The 3D sensor: (a) convoluted FSS (b) complement dielectric layer (c) complement joined together with the FSS (d) complement slid out of the FSS.

TABLE II DIMENSION OF THE FSS

Dimension	p	n	d	b	w	d	h
Value (mm)	26	6.85	4.7	10	2.6	21.7	11

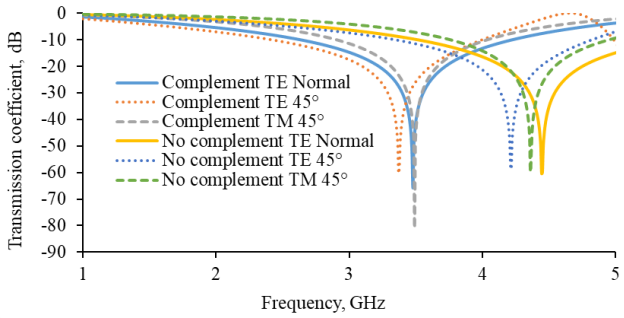


Fig. 8 Simulated S_{21} of 3D sensor with and without the substrate complement

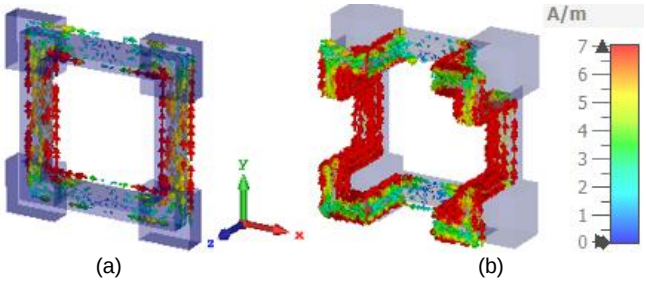


Fig. 9 Surface current distribution on the FSS. (a) 2D (b) 3D, FSS.

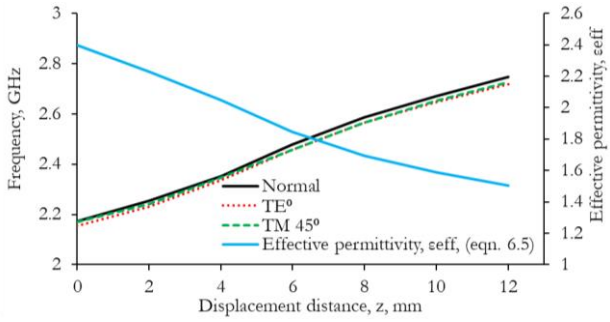


Fig. 10 Simulated effect of displacement on resonance frequency, and the equivalent effective permittivity for the 3D convoluted FSS sensor.

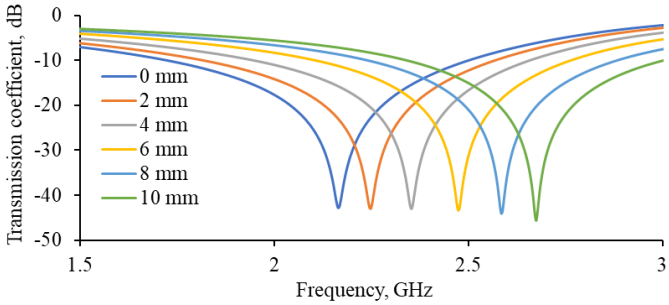


Fig. 11 Simulated S21 results for complement withdrawn distance

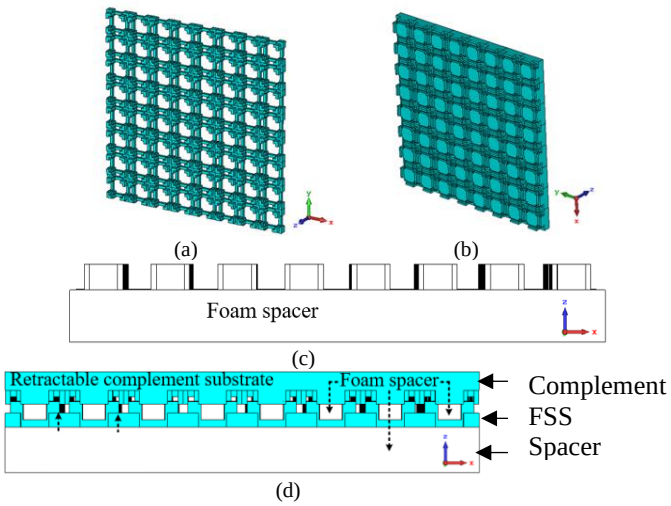


Fig. 12 Full model of the (a) FSS sensor substrate (b) dielectric complement, (c) foam spacer (d) mounting mechanism of the FSS sensor with spacer.

IV. FABRICATION AND MEASUREMNTS

A. Fabrication

The cell unit of dimensions shown in Fig. 7 and Table III was extended to an 8 x 8 array, Fig. 12. Fig. 12(a) and Fig. 12(b) are the convoluted FSS and complement substrate respectively, both 207 mm x 207 mm in size. This size is scalable. Previous work [45] indicates that even a single unit cell can produce transmission selectivity. Five spacers, heights 0 mm to 10 mm at 2 mm intervals were also made. A sample is shown in Fig.12(c). The spacers were used to position the complement at the correct height as illustrated in Fig. 12(d). The fabrication process had two stages, the printing of the polyactide acid (PLA) substrate for the FSS and the complement substrate followed by manual painting of the loops on the FSS substrate. The thermal conductivity of PLA is 0.16 $m^{-1} K^{-1}$ [46], and the glass transition temperature is about 60 °C [47].

The CST models of both the convoluted FSS and complement substrate were exported to .stl file and then sent to Raised 3D printer machine using CURA software for printing. After the FSS substrate was printed, conductive loops were hand painted using RS pro Silver Conductive 186-3600 paint [48], around the cells on the substrate using an artist's painting brush. The fabricated FSS sensor is shown in Fig. 13. The FSS substrate with the painted loops is shown in Fig. 13(a) and (b), the complement substrate in Fig. 13(c) and (d). Fig. 13(e) and (f) show the two parts lock together while Fig. 13(g) and (h) shows a sample of one of the spacers which were cut from polystyrene

Authorized licensed use limited to: UNIVERSITY OF KENT. Downloaded on July 14,2023 at 13:16:53 UTC from IEEE Xplore. Restrictions apply.
© 2023 IEEE. Personal use is permitted, but republication/redistribution requires IEEE permission. See https://www.ieee.org/publications/rights/index.html for more information.

This article has been accepted for publication in IEEE Sensors Journal. This is the author's version which has not been fully edited and content may change prior to final publication. Citation information: DOI 10.1109/JSEN.2023.3289777

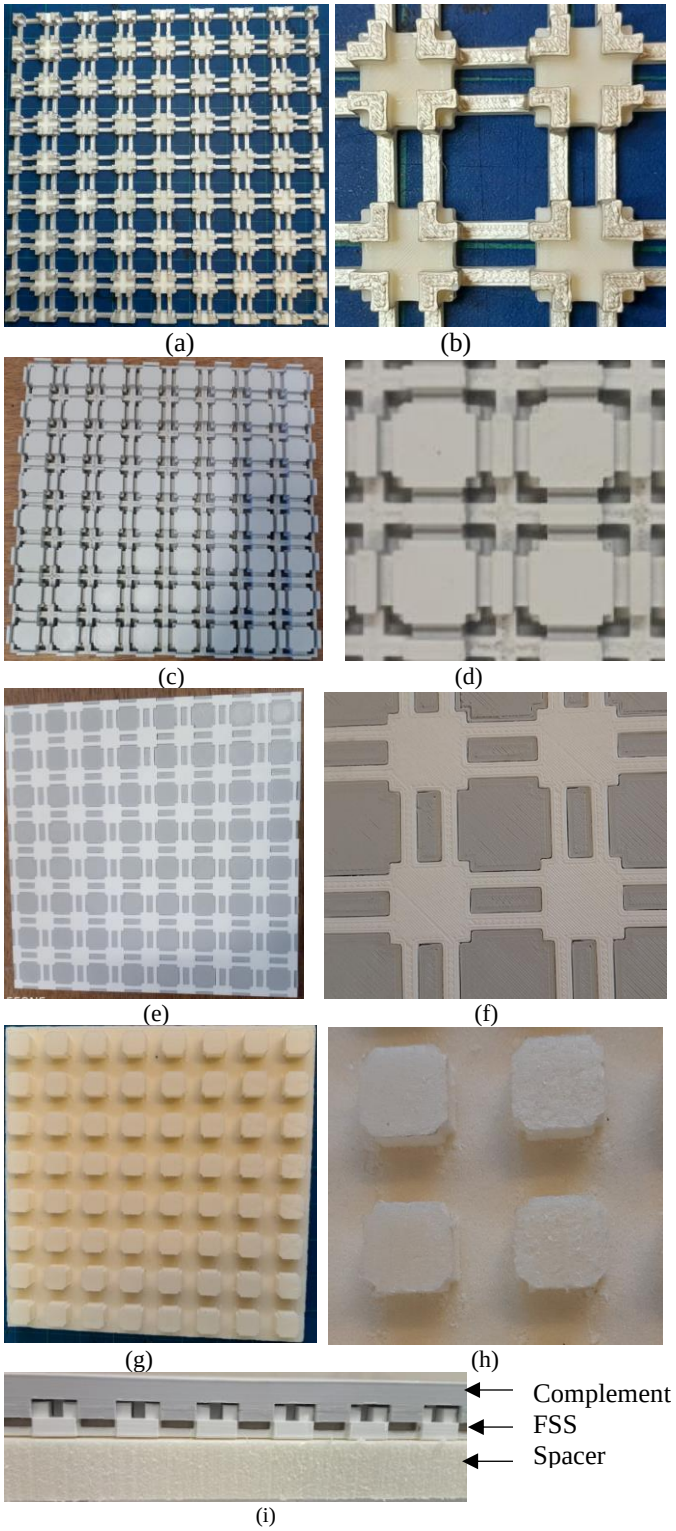


Fig. 13 Fabricated FSS sensor and spacer (a) the printed FSS (b) 4x4 array of the printed FSS showing the painted conductors, (c) and (d) the substrate complement, (e) and (f) FSS fully attached to the complement, (g) and (h) a foam spacer, (i) complement from the FSS using the spacer.

foam blocks using a Denford Router 2600 CNC machine and were used to mimic the substrate complement retraction from the FSS. Polystyrene foam was used because it has relative permittivity closest to air and thus would have minimal effect on the measurements. Fig. 13 (i) is a side view of the FSS positioning using a foam spacer.

B. The Measurements

The FSS sensor's transmission coefficient measurements, S_{21} were conducted as shown in Fig. 14 using Marconi Instruments microwave test set 6204B. Fig. 14(a) shows the measurement set while Fig. 14(b) shows the sensor's testing position. Two R&S®HL050 log-periodic antennas from Rohde & Schwarz GmbH & Co. with a range of 0.85-26.5 GHz, passive gain of 7.5 dBi were placed at 70 cm on either side of the prototype for measurements. The transmission coefficient was normalized using a through calibration against an aperture 210 mm x 210 mm.

The FSS (Fig. 13(a)) was measured first, followed by FSS locked with the complement substrate (Fig. 13(e)). Fig. 15 shows the prototype's transmission response measured without and with the substrate complement. The FSS without the complement resonated at 2.7 GHz with a frequency shift of 0.37% at TE 45º, and 0.74% at TM 45º. The FSS coupled to the complement resonates at 2.16 GHz with 0.4% frequency shift at TE 45º, and 0.9% at TM 45º.

S_{21} measurements were also carried out for the complement substrate displacement distance, z, from 0 mm to 10 mm at normal incidence, Fig. 16. The results show that the resonance frequency progressively shifts to higher frequencies as the complement substrate is gradually withdrawn. Fig.17 shows both the simulated and measured response of the sensor. This behavior is consistent with the linear dependence on z noted in simulation with less than 3.8% deviation observed at any point. The sensor exhibits a high linearity factor R^2 of 0.997 over the measured range. The maximum errors for the TE45 and TM45 frequency shift is just under 1mm, which is the minimum reliable and detectable displacement that could be sensed effectively. The differences between the simulated and measured results could be due to fabrication, measurement errors or potential deviation of the relative permittivity of the printed structure [49][50].

V. Discussion

Table III summarizes the performance of other reported FSS based displacement sensors compared to the proposed design. The proposed sensor differs conceptually and geometrically from [28][29]. [28] is based on the concept of two sliding conductors horizontally, while [29] focuses on the separation of conducting metamaterials in the horizontal plane and the detection occurs through coupling to antenna in the near field. Note that other metamaterial-based sensors [51]– [53] have not been included in the table because they are not FSS based and work differently. They are circuit based and cannot be operated remotely.

The sensor has been optimized to target a resonant frequency that can be measured with the available equipment. However, it can be optimized to any other frequency range within the microwave band. Furthermore, the dynamic range can be optimized as wished or extended further by increasing the length of the conductor of the square loop element in the z-direction (Fig.7). The sensitivity could be increased further by using a complement substrate with a higher dielectric constant. The sensor was fabricated using 3D printing techniques and hand painting of the conductive layers of the FSS. The painting was done manually but could be done using a painting machine

Authorized licensed use limited to: UNIVERSITY OF KENT. Downloaded on July 14,2023 at 13:16:53 UTC from IEEE Xplore. Restrictions apply.
© 2023 IEEE. Personal use is permitted, but republication/redistribution requires IEEE permission. See https://www.ieee.org/publications/rights/index.html for more information.

This article has been accepted for publication in IEEE Sensors Journal. This is the author's version which has not been fully edited and content may change prior to final publication. Citation information: DOI 10.1109/JSEN.2023.3289777



(a) (b)

Fig. 14 The (a) plane wave chamber measurement set up (b) sensor on the measurement set up

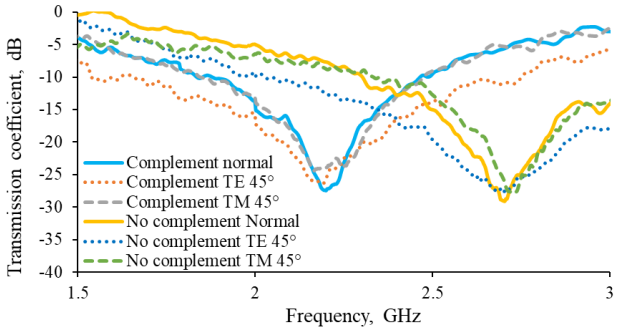


Fig. 15 Measured angle of incidence S_{21} with and without the complement

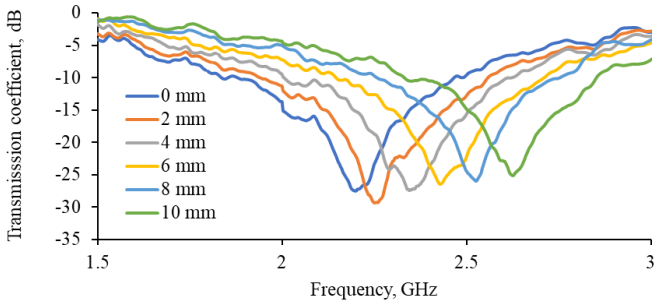


Fig. 16 The S_{21} measurement for TE for the substrate complement withdrawal

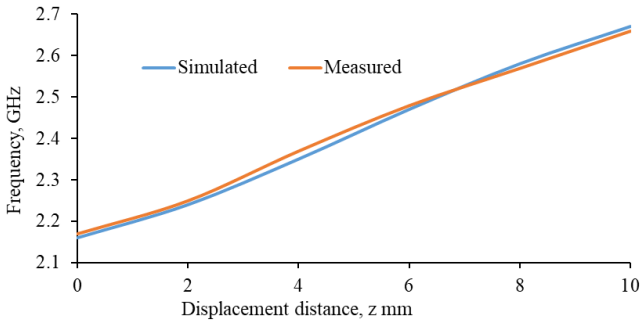


Fig. 17 Curve of resonance frequency, f, versus substrate complement withdrawal distance z of the fabricated sensor

and an electroless plating process. FDM printing and PLA were employed due to their in-house availability. However, this technique has limitations such as the 0.2 mm fabrication accuracy and the potential deformation of PLA for temperatures higher than 60 °C [27]. To operate at higher temperatures or to achieve higher resolution, other fabrication techniques and materials could be employed. The proposed sensor is ideal for instances requiring real-time monitoring of structural changes such as detection of movement or cracks due to deformation

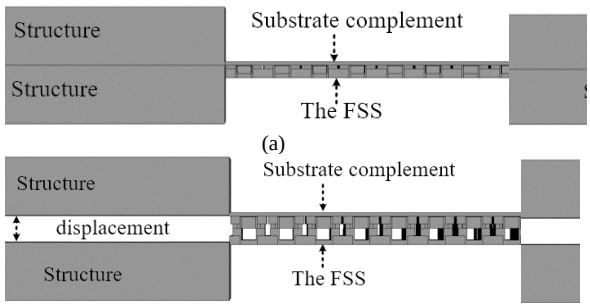


Fig. 18 Potential conceptual arrangement of the structural displacement sensor (a) before displacement, and (b) after displacement

TABLE III COMPARISON OF THE PROPOSED DESIGN WITH THE REPORTED FSS BASED SENSING DESIGNS

Parameters	References		
	[28]	[29]	This work
Frequency (GHz)	10	0.4	2.0
Sensitivity (GHz/mm)	0.326	0.008	0.052
Geometry	2D	2D	3D
Dynamic range (mm)	5	7	10
Sensor type	FSS	Meta material	FSS
Polarization	Single	Single	Dual
Complement structures	No	No	Yes
Unit Cell size	0.4λx0.4λ	0.07λx0.07 λ	0.2λx0.2λ
Field operation	Far field	Near field	Far field

in a civil structure. It could also be used to detect land deformation because of volcanic activity or in earthquake monitoring and prediction. The displacement sensor can be integrated with any structure as illustrated in Fig. 18. Even though measurements were consistent for distances around the setup FSS and TX/RX, if different distances or different TX/RX antennas were to be used, it would be recommended to recalibrate the sensor. In addition, if the antennas are to be placed further away, a larger sensor may need to be used. The movement in the structure from an initial state, Fig.18(a), to Fig. 18(b) leads to a change in the state of the FSS sensor attached to the structure. The initial state of the structure is a solid block (Fig. 18(a)) with the FSS protected by the dielectric layers, which is ideal for external applications.

VI. Conclusion

A novel FSS-based displacement wireless sensor based on a complementary dielectric has been demonstrated. The sensor uses a substrate complement to modify the transmission response of an FSS as the complement is removed in the z-axis. It operates in a frequency range between 2.0 GHz and 2.8 GHz and has achieved a 0.052 GHz/mm sensitivity and 12 mm dynamic range, and has a dimension of 207 mm by 207 mm. The range of the sensor can be extended using 3D convoluted techniques described here, resulting in a new 3D convoluted FSS sensor. Extending the sensor in 3D also improves its angle of incidence behavior and increases the range of the sensor. The FSS structures developed are based on a modified square loop FSS element, and inherently dual polarized. In terms of sensor operation, the withdrawable dielectric substrate changes the effective permittivity and, thus, the capacitance of the FSS array. The FSS sensor provides displacement sensing up to 0.1λ, which can be extended if required.

The sensor has application in wireless monitoring of

Authorized licensed use limited to: UNIVERSITY OF KENT. Downloaded on July 14,2023 at 13:16:53 UTC from IEEE Xplore. Restrictions apply.
© 2023 IEEE. Personal use is permitted, but republication/redistribution requires IEEE permission. See https://www.ieee.org/publications/rights/index.html for more information.

This article has been accepted for publication in IEEE Sensors Journal. This is the author's version which has not been fully edited and content may change prior to final publication. Citation information: DOI 10.1109/JSEN.2023.3289777

displacement. The technique could also have applications in reconfigurable FSS and metasurfaces using an electromechanical process to separate the complementary dielectric layers. The FFF process used in the fabrication of the device offers a reduction in material cost, labour as well as manufacturing time. The fabrication process can also be scaled up.

ACKNOWLEDGMENT

The authors would like to thank Mr. A. Mendoza, Mr. Julien Soosaipillai and Mr. Colin Cresser and Keith Greenhow for their assistance in fabrication and measurements. This work was funded by the EPSRC grant titled Low-Profile Ultra-Wideband WideScanning Multi-Function Beam-Steerable Array Antennas (EP/S005625/1) and the Royal Society - International Exchanges 2019 Cost Share (NSFC) (Ref: IEC\NSFC\191780).

REFERENCES

[1] B. A. Munk, Frequency Selective Surfaces: Theory and Design, Chichester: John Wiley & Sons, Inc., 2000.

[2] E. A. Parker, "The Gentleman's Guide To Frequency Selective Surfaces," in *17th Q.M.W. Antenna Symposium*, London, April 1991.

[3] D. F. Pieper and K. M. Donnell, "Application of frequency selective surfaces for inspection of layered structures," in *IEEE International Instrumentation and Measurement Technology Conference (I2MTC) Proceedings*, Pisa, Italy, 2015.

[4] P. Callaghan, E. A. Parker and R. J. Langley, "Influence of supporting dielectric layers on the transmission properties of frequency selective surfaces," *IEE Proceedings-H*, vol. 138, no. 5, pp. 448 – 454, 1991.

[5] L. E. Comtesse, R. J. Langley, E. A. Parker and J. C. Vardaxoglou, "Frequency Selective Surfaces in Dual and Triple Band Offset Reflector Antennas," in *17th European Microwave Conference*, Rome, Italy, 1987.

[6] S. Chakravarty, R. Mittra and N. Williams, "Application of a microgenetic algorithm (MGA) to the design of broadband microwave absorbers using multiple frequency selective surface screens buried in dielectrics," *IEEE Transactions on Antennas and Propagation*, vol. 50, no. 3, pp. 284 - 296, 2002.

[7] F. Costa and A. Monorchio, "A Frequency Selective Radome With Wideband Absorbing Properties," *IEEE Transactions on Antennas and Propagation*, vol. 60, no. 6, pp. 2740 - 2747, 2012.

[8] C.-C. Chang, R.-H. Lee and T.-Y. Shih, "Design of a Beam Switching/Steering Butler Matrix for Phased Array System," *IEEE Transactions on Antennas and Propagation* , vol. 58, no. 2, pp. 367 - 374, 2010.

[9] A. A. Dewani, S. G. O'Keefe, D. V. Thiel and A. Galehdar, "Window RF Shielding Film Using Printed FSS," *IEEE Transactions on Antennas and Propagation*, vol. 66, no. 2, pp. 790 - 796, 2018.

[10] L. Zhang, Q. Wu and T. A. Denidni, "Electronically Radiation Pattern Steerable Antennas Using Active Frequency Selective Surfaces," *IEEE Transactions on Antennas and Propagation*, vol. 61, no. 12, pp. 6000 - 6007, 2013.

[11] B. Liang, B. Sanz-Izquierdo, E. A. Parker and J. C. Batchelor, "Cylindrical Slot FSS Configuration for Beam-Switching Applications," *IEEE Transactions on Antennas and Propagation*, vol. 63, no. 1, pp. 166 - 173, 2015.

[12] S. Soltani, P. S. Taylor, E. A. Parker and J. C. Batchelor, "Popup Tunable Frequency Selective Surfaces for Strain Sensing," *IEEE Sensors Letters*, vol. 4, no. 4, 2020.

[13] B. G. Xia, D. H. Zhang, J. Meng, J. Huang, C. F. Yao and J. S. Zhang, "Terahertz FSS for space borne passive remote sensing application," *Electronics Letters* , vol. 49, no. 22, p. 1398–1399, 2013.

[14] S. Y. Jun, B. S. Izquierdo and E. A. Parker, "Liquid Sensor/Detector Using an EBG Structure," *IEEE Transactions on Antennas and Propagation*, vol. 67, no. 5, pp. 3366 - 3373, 2019.

[15] Al-Naiba, I. A, Ibraheem, C. Jansen and M. Koch, "Thin-film sensing with planar asymmetric metamaterial resonators," *Appl. Phys. Lett.*, vol. 93, no. 8, pp. 1-3, 2008.

[16] D. Hasan and C. Lee, "Hybrid Metamaterial Absorber Platform for Sensing of CO2 Gas at Mid-IR," *Advanced Science*, vol. 5, no. 5, pp. 1-13, 2018.

[17] D. Pieper, K. M. Donnell, O. Abdelkarim and M. A. ElGawady, "Embedded FSS sensing for structural health monitoring of bridge columns," in *2016 IEEE International Instrumentation and Measurement Technology Conference Proceedings*, Taipei, Taiwan, 2016.

[18] C. Debus and P. H. Bolivar, "Frequency selective surfaces for high sensitivity terahertz sensing," *Appl. Phys. Lett.*, vol. 91, no. 18, pp. 1-3, 2007.

[19] A. M. J. Marindra and G. Y. Tian, "Chipless RFID sensor for corrosion characterization based on frequency selective surface and feature fusion," *Smart Materials and Structures*, vol. 29, pp. 1-10, 2020.

[20] G. Díaz, N. N. Cano and R. Álvarez, "Determination of the Real Cracking Moment of Two Reinforced Concrete Beams Through the Use of Embedded Fiber Optic Sensors," *Sensors*, vol. 20, no. 3, pp. 1-25, 2020 .

[21] D. S. Nyce, Linear Position Sensors: Theory and Application, Hoboken: John Wiley & Sons, Inc., 2004.

[22] A. K. Horestani, Z. Shaterian and M. Mrozowski, "High Dynamic Range Microwave Displacement and Rotation Sensors Based on the Phase of Transmission in Groove Gap Waveguide Technology," IEEE Sensors Journal, vol. 22, no. 1, pp. 182 - 189, 2022.

[23] Z. Mehrjoo, A. Ebrahimi and K. Ghorbani, "Microwave Resonance-Based Reflective Mode Displacement Sensor With Wide Dynamic Range," IEEE Transactions on Instrumentation and Measurement, vol. 71, 2022.

[24] J. Muñoz-Enano, P. Vélez, L. Su, M. Gil-Barba and F. Martín, "A Reflective-Mode Phase-Variation Displacement Sensor," IEEE Access , vol. 8, pp. 189565 - 189575, 2020.

[25] M. Joodaki and M. Rezaee, "Coplanar Waveguide (CPW) Loaded With an Electromagnetic Bandgap (EBG) Structure: Modeling and Application to Displacement Sensor," *IEEE Sensors Journal*, vol. 16, no. 9, pp. 3034 - 3040, 2016.

[26] J. Basseri and M. Joodaki, "An Angular Displacement Sensor With a Curved Two-Metal-Layer CPW Loaded by an EBG Structure," *IEEE Sensors Journal*, vol. 18, no. 6, pp. 2335 - 2341, 2018.

[27] S.-D. Jang, B.-W. Kang and J. Kim, "Frequency selective surface based passive wireless sensor for structural health monitoring," *Smart Materials And Structures*, vol. 22, no. 2, pp. 1-8, 2013.

[28] J.-J. Zhang, B. Wu, Y.-T. Zhao, L. Song, H.-R. Zu, R.-G. Song and D.-P. He, "Two-Dimensional Highly Sensitive Wireless Displacement Sensor With Bilayer Graphene-Based Frequency Selective Surface," *IEEE Sensors Journal*, vol. 21, no. 21, pp. 23889-23897, 2021.

[29] B. Ozbey, E. Unal, H. Ertugrul, O. Kurc, C. M. Puttlitz, V. B. Erturk, A. Altintas and H. V. Demir, "Wireless Displacement Sensing Enabled by Metamaterial Probes for Remote Structural Health Monitoring," *Sensors*, vol. 14, no. 1, pp. 1691-1704, 2014.

[30] R. S. Anwar, L. Mao and H. Ning, "Frequency Selective Surfaces: A Review," *MPDI Applied Sciences*, vol. 8, no. 9, pp. 1-47, 2018.

[31] Philips, B., Parker, Edward A., Langley, Richard J. (1993) Finite curved frequency selective surfaces. Electronics Letters, 29 (10). pp. 882-883. ISSN 0013-5194.

[32] S. N. Azemi, K. Ghorbani and W. S. T. Rowe, "3D Frequency Selective Surfaces," Progress In Electromagnetics Research C, vol. 29, pp. 191–203, 2012.

[33] K. Tao, B. Li, Y. Tang, M. Zhang and Y. Bo, "Analysis and implementation of 3D bandpass frequency selective structure with high frequency selectivity," *ELECTRONICS LETTERS* , vol. 53, no. 5, p. 324–326, 2017.

Authorized licensed use limited to: UNIVERSITY OF KENT. Downloaded on July 14,2023 at 13:16:53 UTC from IEEE Xplore. Restrictions apply.
© 2023 IEEE. Personal use is permitted, but republication/redistribution requires IEEE permission. See https://www.ieee.org/publications/rights/index.html for more information.

This article has been accepted for publication in IEEE Sensors Journal. This is the author's version which has not been fully edited and content may change prior to final publication. Citation information: DOI 10.1109/JSEN.2023.3289777

[34] B. Al-Juboori, J. Zhou, Y. Huang, M. Hussein, A. Alieldin, W. J. Otter, D. Klugmann and S. Lucyszyn, "Lightweight and Low-Loss 3-D Printed Millimeter-Wave Bandpass Filter Based on Gap-Waveguide," *IEEE Access*, vol. 7, pp. 2624 - 2632, 2018.

[35] J. H. Barton, C. R. Garcia, E. A. Berry, R. Salas and R. C. Rumpf, "3-D Printed All-Dielectric Frequency Selective Surface With Large Bandwidth and Field of View," *IEEE Transactions on Antennas and Propagation*, vol. 63, no. 3, pp. 1032 - 1039, 2015.

[36] B. Sanz-Izquierdo and E. A. Parker, "3-D Printing of Elements in Frequency Selective Arrays," *IEEE Transactions On Antennas And Propagation*, vol. 62, no. 12, pp. 6060-6066, 2014.

[37] S. Dey and S. Dey, "Conformal Miniaturized Angular Stable Triband Frequency Selective Surface for EMI Shielding," IEEE Transactions on Electromagnetic Compatibility, vol. 64, no. 4, pp. 1031 - 1041, 2022.

[38] T. Li, D. Li, P. Qin, Y. Fan, Y. Gu, P. Zuo, W. E. I. Sha and E. Li, "A Novel Miniaturized Strong-Coupled FSS Structure With Excellent Angular Stability," IEEE Transactions on Electromagnetic Compatibility, vol. 63, no. 1, pp. 38 - 45, 2021.

[39] E. Parker, A. E. sheikh and A. d. C. Lima, "Convoluted frequency-selective array elements derived from linear and crossed dipoles," 1EE PROCEEDINGS-H, vol. 140, no. 5, p. 378 – 380, 1993.

[40] Tractus3D, "FDM 3D printing – Fused Deposition," Tractus 3D, 01 10 2021. [Online]. Available: https://tractus3d.com/knowledge/learn-3d-printing/fdm-3d-printing/. [Accessed 01 10 2021].

[41] S. Y. Jun, A. Elibiary, B. Sanz-Izquierdo, L. Winchester, D. Bird and A. McCleland, "3-D Printing of Conformal Antennas for Diversity Wrist Worn Applications," *IEEE Transactions on Components, Packaging And Manufacturing Technology*, vol. 8, no. 12, pp. 2227-2235, 2018.

[42] I. Anderson, "On the Theory of Self-Resonant Grids," *The Bell System Technical Journal*, vol. 54, no. 10, pp. 1725 - 1731, 1975.

[43] N. Marcuvitz, Waveguide Handbook, Exeter: Short Run Press, 1986.

[44] P. Callaghan and E. A. Parker, "Element dependency in dielectric tuning of frequency selective surfaces," *Electronics Letters*, vol. 28, no. 1, pp. 42 – 44, 1992.

[45] E.A. Parker, J.-B. Robertson, B. Sanz-Izquierdo and J. C. Batchelor, "Minimal size FSS for long wavelength operation," *Electronics Letters*, vol. 44, no. 6, p. 394 – 395, 2008.

[46] I. Blanco, G. Cicala, G. Recca and C. Tosto, "Specific Heat Capacity and Thermal Conductivity Measurements of PLA-Based 3D-Printed Parts with Milled Carbon Fiber Reinforcement," Entropy, vol. 24, no. 5, 2022.

[47] J. Suder, Z. Bobovsky, M. Safar, J. Mlotek, M. Vocetka and Z. Zeman, "Experimental Analysis Of Temperature Resistance Of 3d Printed Pla Components," *MM Science Journal*, pp. 4322-4327, 2021.

[48] "RS PRO Liquid Conductive Paint," RS, 10 06 2021. [Online]. Available: https://uk.rs-online.com/web/p/adhesives/1863600/. [Accessed 10 06 2021].

[49] S. Moscato, R. Bahr, T. Le, M. Pasian, M. Bozzi, L. Perregrini and M. M. Tentzeris, "Infill-Dependent 3-D-Printed Material Based on NinjaFlex Filament for Antenna Applications," *IEEE Antennas and Wireless Propagation Letters*, vol. 15, pp. 1506 - 1509, 2016.

[50] A. Goulas, S. Zhang, D. A. Cadman, J. Järveläinen, V. Mylläri, W. G. Whittow, J. (. C. Vardaxoglou and D. S. Engstrøm, "The Impact of 3D Printing Process Parameters on the Dielectric Properties of High Permittivity Composites," *MPDI Designs*, vol. 3, no. 4, pp. 1-10, 2019.

[51] M. Abdolrazzaghi and M. Daneshmand, "Multifunctional Ultrahigh Sensitive Microwave Planar Sensor to Monitor Mechanical Motion: Rotation, Displacement, and Stretch," *Sensors*, vol. 20, no. 4, pp. 1-19, 2020.

[52] A. K. Horestani, C. Fumeaux, S. F. Al-Sarawi and D. Abbott, "Displacement Sensor Based on Diamond-Shaped Tapered Split Ring Resonator," *IEEE Sensors Journal*, vol. 13, no. 4, pp. 1153 - 1160, 2013.

[53] A. K.Horestani, J. Naqui, Z. Shaterian, D. Abbott, C. Fumeaux and F. Martín, "Two-dimensional alignment and displacement sensor based on movable broadside-coupled split ring resonators," *Sensors and Actuators A: Physical*, p. 18–24, 2014.



Peter Njogu completed a Ph.D. in electronic engineering from the University of Kent, Canterbury, U.K. His research interests include wearable antennas, multiband antennas, FSS, millimetre wave antennas and 3D printed antennas and sensors.



Benito Sanz Izquierdo received the B.Sc. from ULPGC (Spain), and the M.Sc. and Ph.D. degrees from the University of Kent, U.K. He was Research Associate with the School of Engineering, University of Kent, in 2013, became lecturer in Electronic Systems and, in 2018, Senior Lecturer. In 2012, he worked for Harada Industries Ltd where he developed novel antennas for the automotive industry. His research interests are multiband antennas, wearable electronics, additive manufacturing (3D printing), substrate integrated waveguides components, metamaterials, electromagnetic band-gap structures, frequency selective surfaces and reconfigurable devices.



Zhijiao Chen (S'13-M'14) received BSc from Beijing University and Posts and Telecommunications in 2010, Ph.D. degree from Queen Mary University of London in 2014 and join the school of electronic engineering in Beijing University and Posts and Telecommunications as a Lecturer in 2014. Dr. Chen was secondment to Ace-Axis Wireless Technology Laboratories Ltd (Essex, UK) in 2012, and joined Northeastern University (Boston, MA) as a visiting student in 2013. She was the receipts of the Best Paper Award in iWAT 2013 (Karlsruhe, Germany), 3rd Prize Student Paper Competition in APS/URSI 2013 (Orlando, FL), TICRA Travel Grant in EuCAP 2014 (Hague, Netherland), and 3rd Place in QMUL Three-Minute Thesis (3MT) Competition Final 2014 (London, UK). Her research interests include dielectric resonator antennas, millimeter wave antennas and 3D printed antennas.



Edward (TED) A. Parker received the M.A. degree in physics and the Ph.D. degree in radio astronomy from the St. Catharine's College, University of Cambridge, Cambridge, U.K in 1968, respectively. He was appointed as a Reader with the University of Kent, Canterbury, U.K., in 1977, where he has been a Professor of Radio Communications, since 1987. He is currently a Professor Emeritus with the University of Kent. He established the Electronics Laboratory, Antennas Group, and University of Kent. He is a member of the Livery of the Worshipful Company of Scientific Instrument Makers, London, U.K. His current research interests include the application of frequency selective surfaces and the study and overhaul of antique clocks. He is a member of the Institution of Engineering and Technology.

Authorized licensed use limited to: UNIVERSITY OF KENT. Downloaded on July 14,2023 at 13:16:53 UTC from IEEE Xplore. Restrictions apply.
© 2023 IEEE. Personal use is permitted, but republication/redistribution requires IEEE permission. See https://www.ieee.org/publications/rights/index.html for more information.